



# Investigation of the structural and optical properties of $\text{Sb}_2\text{S}_3$ /PVA/PVP nanocomposites blended sheets for optoelectronic applications

N. M. Farrage<sup>1</sup> · Nahed H. Teleb<sup>2</sup> · W. A. Abd El-Ghany<sup>2</sup>

Received: 3 November 2023 / Accepted: 14 December 2023 / Published online: 27 January 2024  
© The Author(s) 2024

## Abstract

$\text{Sb}_2\text{S}_3$  chalcogenide Nanopowder was prepared at low temperatures using the chemical co-precipitation method. PVA/PVP polymeric sheets have been prepared with a constant ratio of 2:1 as a host matrix to incorporate  $\text{Sb}_2\text{S}_3$  NPS with a ratio of 0, 1, 3, and 5 wt% via solution casting technique. The X-ray diffraction (XRD) pattern revealed that the prepared  $\text{Sb}_2\text{S}_3$  powder belongs to an orthorhombic crystalline structure as a major phase, with a crystal size of 24 nm. The microstructure of the powder as well as 5 wt%  $\text{Sb}_2\text{S}_3$ /PVA/PVP was investigated using the transmission electron microscope. The Fourier transform infrared spectra of the prepared sheets revealed the success of the interaction between the filler  $\text{Sb}_2\text{S}_3$  material with the PVA/PVP as a polymer host matrix. The transmission and reflection spectra of the polymeric  $\text{Sb}_2\text{S}_3$  /PVA/PVP sheets measured in the wavelength range 200–2500 nm have been used to calculate the optical band gap energy and refractive index as a function in the  $\text{Sb}_2\text{S}_3$  wt%. The Tauc model and the absorption spectrum fitting model were employed to accurately determine the variation of the optical band gap value with  $\text{Sb}_2\text{S}_3$  filler percent. Wemple-DiDomenico single-oscillator and Spitzer-Fan, models were applied to analyze the refractive index as a function of the  $\text{Sb}_2\text{S}_3$  filling wt%, whereby the dispersion parameters,  $E_d$ ,  $E_o$  as well as the optical high-frequency dielectric constant,  $\epsilon_L$  carrier concentration to the effective mass ratio,  $N/m^*$  were evaluated. A graphical representation of the optical conductivity was also present. The obtained data indicate the possibility of using the prepared  $\text{Sb}_2\text{S}_3$ /PVA/PVP nanocomposite sheets for optoelectronic applications and optical devices.

**Keywords**  $\text{Sb}_2\text{S}_3$ /PVA/PVP · Nanopowder · XRD · Optical band gap · The absorption spectrum fitting model (ASF) · Refractive index

---

✉ W. A. Abd El-Ghany  
wa.abdel-ghany@nrc.sci.eg

<sup>1</sup> Spectroscopy Department, Physics Research Institute, National Research Center, El-Bohoos St., DokkiCairo 12622, Giza, Egypt

<sup>2</sup> Electron Microscopy and Thin Films Department, Physics Research Institute, National Research Center, El-Bohoos Str., Dokki 12622, Giza, Egypt

## 1 Introduction

Mixing different polymer materials with an appropriate quantity is considered at present one of the most important ways to design new materials with a wide diversity of physical properties suitable for different technological applications (Zidan et al. 2019, 2016; Abdelrazek et al. 2010; Elashmawi et al. 2014). Polyvinyl alcohol (PVA) is considered widely used as an artificial polymer due to its excellent physical and chemical e.g. its solubility in water, high transparency, non-toxicity, in addition to its high flexibility (Ben Doudou et al. 2014; Kochi et al. 2019). Many studies demonstrated the novel and distinctive properties of embedding different types of nanoparticles (NPs) in PVA such as CdS (Heiba et al. 2017), ZnO (Hemalatha et al. 2014),  $Zn_{1-x}Mg_xO$  (Heiba and Mohamed 2019), PbS (Abdullah et al. 2015a) and  $Zn_{1-x}Cu_xS$  (Mohamed et al. 2018), etc. This is due to the combination of polymer matrices' inherent characteristics, such as ease of processing, flexibility, and high mechanical strength in addition to the unique optical and chemical properties of the NPs that make them highly desirable for various applications. It is also possible to blend PVA with one polymer such as carboxymethyl cellulose (CMC) (Heiba et al. 2021a), polyethylene glycol (PEG) (Heiba et al. 2022), Poly(MethylMethAcrylate) (PMMA) (Alsaad et al. 2021) and Polyvinylpyrrolidone (PVP) (El-naggar et al. 2021, 2022a) or with two polymers, as in PVA/PVP/PEG (El-naggar et al. 2022b), PVA/PMMA/PAAm (Polyacrylamide) (Mohammed Kadim et al. 2023) and PVA/CMC/PEG (Li et al. 2019; Fewaty et al. 2016). The polymer blends that were produced exhibit different behavior when compared to their constituents (El-naggar et al. 2021).

PVP also has similar characteristics to PVA besides it contains a pyrrolidone ring functional group that promotes strong adhesion to the filling material (Badawi 2021). The bond constancy that occurs between both PVA and PVP when blended was attributed to the interaction between the OH group of PVA and the C=O group of PVP (Rajesh et al. 2019a; Baraker and Lobo 2016). Mixing the two polymers together is subject to a lot of interesting scientific research to maximize their physical properties and determine the most beneficial for its uses (Badawi 2020; Uma Maheshwari et al. 2017; Elashmawi and Abdel Baieth 2012; Sudha Kamath et al. 2015). It has been reported that mixing of PVA/PVP with increasing PVP concentration ratio reflects a reduction in the crystalline nature of the polymer blend and enhances its permeability and adhesive properties to be used as a biomaterial for cell culture (Hatta et al. 2005). It has been reported that PVA/PVP polymer mixed with a ratio of 80:20 exhibited better electrical properties than the other ratios studied (Helberg et al. 2020).

Furthermore, the combination of blended polymer with a foreign metal oxide forms a Nano-composite matrix providing a new class of material characterized by promising physical and optical properties suitable for electronic and optoelectronic devices (Rajesh et al. 2019a; Bdewi et al. 2016; Abd El-Kader et al. 2021; Al-Ramadhan et al. 2016). The addition of Nano-metal elements such as silver (Ag) or gold (Au) also reflects an improvement in the optical properties of such blends (Sudheesh et al. 2011). Moreover, it is easy to combine ionic metal oxide nanoparticles like CuO with polymers to create composites with unique physicochemical properties (Abd El-Kader et al. 2021). These nanoparticles can have antimicrobial effects when used at a certain dose due to their high surface area and crystalline structures.

Additionally, metal chalcogenides have also received great attention due to their unique optical and electronic properties, which can be selected as fillers in PVA/PVP polymeric mixtures for applicable different technological applications. For example, the structural and

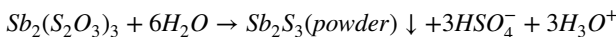
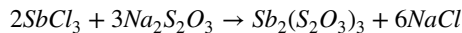
optical properties of  $\text{Ag}_2\text{S}$  (Aziz et al. 2017a),  $\text{SnS}$  (Badawi 2020), and,  $\text{SnS}_2/\text{Fe}$  (El-nagar et al. 2022a) chalcogenides material embedded in the PVA/PVP host matrix have been reported. In this context,  $\text{Sb}_2\text{S}_3$  material of optical band gap energy of 1.7 eV is a widely demonstrated promising chalcogenide compound in many fields of application e.g. photo-catalysts, solar cells, photonic integrated circuits, etc. (Arumugam et al. 2018a, 2018b). However, to the best of our knowledge, there is no report yet concerning the characterization of  $\text{Sb}_2\text{S}_3$  embedded in a PVA/PVP mixture as a host matrix.

The study aims to investigate the structural and optical properties of  $\text{Sb}_2\text{S}_3/\text{PVA}/\text{PVP}$  composites while clarifying to what extent the optical properties of the PVA/PVP host matrix are affected by adding  $\text{Sb}_2\text{S}_3$  in varying proportions, to search for the possibility of obtaining the properties required for appropriate for optoelectronic applications.

## 2 Experimental technique

### 2.1 Preparation of $\text{Sb}_2\text{S}_3$ nanoparticles

$\text{Sb}_2\text{S}_3$  powder has been prepared by the chemical co-precipitation method as follows (Salem and Selim 2001). In a 100 mL beaker; 650 mg of  $\text{SbCl}_3$  dissolved in 2.5 mL of acetone, followed by adding 25 mL of 1 M sodium thiosulfate ( $\text{Na}_2\text{S}_2\text{O}_3 \cdot 5\text{H}_2\text{O}$ ) maintained at 10 °C, after that adding 70 mL of double distilled water also kept at 10°C. A clear solution of pH 5 was obtained, stirred well for a few minutes and maintained in a refrigerator for the next day. A granulated powder of a red–orange color precipitated at the bottom of the beaker, was collected, washed well with distilled water several times, and dried at a temperature of 60° until a constant weight was obtained. The chemical equations reaction for this process is as follows:



### 2.2 Preparation of $\text{Sb}_2\text{S}_3/\text{PVA}/\text{PVP}$ Nano composites sheets and measurements

Separate PVA and PVP solutions were prepared by dissolving 6 wt% of each in distilled water and stirred using a magnetic stirrer at 90 °C for 2 h until a clear solution was obtained. Stock solution of PVA/PVP was prepared by mixed PVA: PVP of ratio 2:1 at room temperature and stirred continuously for an hour to get a clear homogenous solution. Separate solutions of the above mixed PVA/PVP were filled by different 1, 3, and 5 wt% of  $\text{Sb}_2\text{S}_3$  powder prepared according to Eq. (1). Each solution was ultra-sonicated for 20 min, then poured onto a petri dish, and kept in an oven for 24 h at 40 °C to prepare polymeric sheets. Figure 1a, b shows the schematic diagram for the preparation of precipitated  $\text{Sb}_2\text{S}_3$  powder (a), and  $\text{Sb}_2\text{S}_3$  NPs/PVA/PVP polymeric sheets (b).

The structural characterization of the prepared  $\text{Sb}_2\text{S}_3$  powder at room temperature was performed using X-ray diffraction (Type a Bruker D-8 advance X-ray diffractometer). The diffractometer worked at 40 kV and 40 mA using  $\text{CuK}\alpha_1$  radiation of wavelength  $\lambda=0.1541$  nm in the  $2\theta$  range 10°–75°. The microstructure of the powder was investigated using a transmission electron microscope (Type JEOL-JEM 1230) operating at 120 kV. Transmission electron

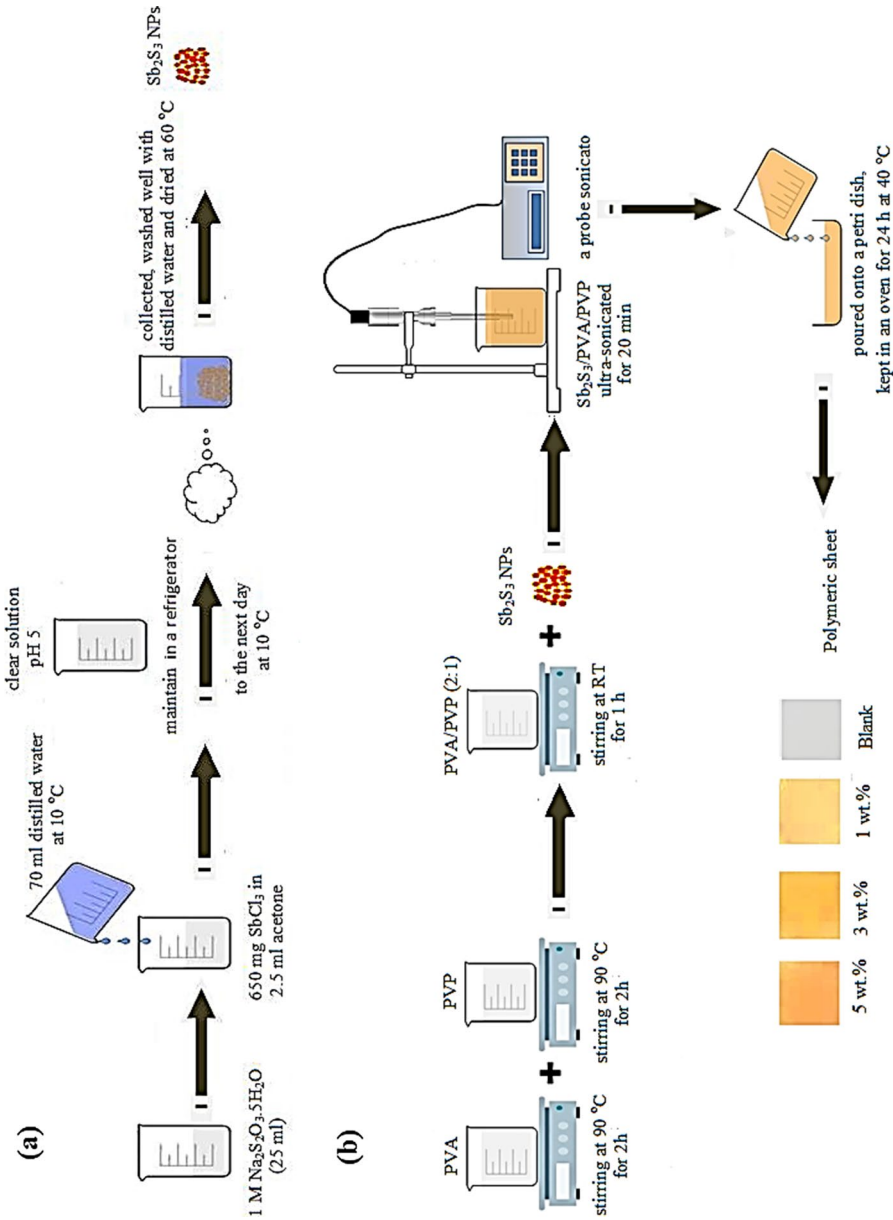


**Fig. 1** A schematic diagram for **a** the prepared  $Sb_2S_3$  powder, and **b** the solution casting plan to prepare  $Sb_2S_3$  NPs/PVA/PVP polymeric sheets

micrograph of a thin polymer sheet of thickness 30 nm for PVA/PVP sample filled with  $\text{Sb}_2\text{S}_3$  by a ratio of 5 wt%, prepared by cutting a piece of polymer sheet using a glass knife of ultramicrotome (Type Leica EM UC6) was investigated using the TEM device. The Fourier transform (FTIR) measurement of the prepared composite sheets has been performed to detect the various types of bond stretching and vibrations in the prepared composite sheets using a spectrometer VERTEX 80 (Bruker Corporation, Germany) in conjunction with a Platinum Diamond ATR, which uses a diamond disc as the internal reflection element in the wavenumber range from 4000 to 500  $\text{cm}^{-1}$ . The transmission and reflection spectra of the prepared composite sheets were carried out at room temperature using a double-beam UV–visible–NIR spectrophotometer (Type Jasco, V-570, UV–Vis–NIR) in the wavelength range from 190 to 2500 nm.

### 3 Results and discussion

#### 3.1 Structural characterization

Figure 2 shows the X-ray diffraction of the  $\text{Sb}_2\text{S}_3$  powder prepared by the co-precipitation method. The figure depicts that the prepared powder exhibits a polycrystalline structure corresponding to  $\text{Sb}_2\text{S}_3$  as a major orthorhombic phase (JCPDS card No: 87–1135). However, three minor additional peaks were noticed; these peaks are indexed as (113), (313), and (402) corresponding to  $\text{Sb}_9.8\text{S}_{15}$  (JCPDS card No: 77–2467), besides two other faint peaks indexed as (111), and (022) corresponding to antimony oxide  $\text{Sb}_2\text{O}_3$  as a minor orthorhombic phase (JCPDS card No: 74–1725). The  $2\theta$  values of the observed peaks and interplaner distance as well as the corresponding ( $hkl$ ) are listed in Table 1. The lattice parameters  $a$ ,  $b$ , and  $c$  for the present major orthorhombic phase have been calculated using the reflection (022), (700), and (004) planes via the equation (Cullity 1978):

$$\frac{1}{d_{hk\uparrow}^2} = \frac{h^2}{a^2} + \frac{k^2}{b^2} + \frac{\uparrow^2}{c^2} \quad (1)$$

**Fig. 2** The X-ray diffraction pattern of the precipitated  $\text{Sb}_2\text{S}_3$  powder. (M denoted  $\text{Sb}_{9.5}\text{S}_{15}$  monoclinic phase, while, O denoted  $\text{Sb}_2\text{O}_3$  orthorhombic phase)

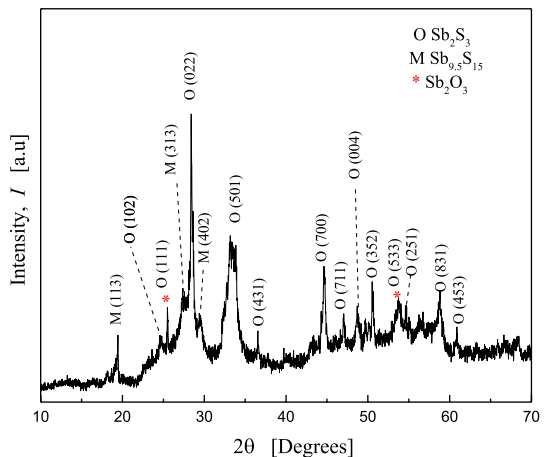


**Table 1** The  $2\theta$  values of X-ray peaks, d-spacing and the corresponding ( $hkl$ )

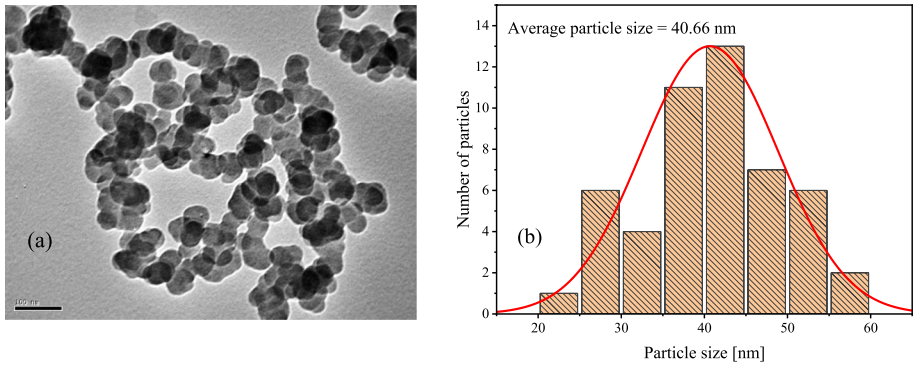
2 $\theta$ [Degrees]		Interplaner distance (d) [nm]		$Hkl$
Observed	JCPDS	Observed	JCPDS	
19.269	19.209	4.60264	4.6168	113
24.727	24.626	3.59761	3.6121	102
25.486	25.454	3.49215	3.4965	111
27.547	27.504	3.23539	3.2404	313
28.396	28.496	3.14054	3.1297	022
29.396	29.415	3.03595	3.034	402
33.865	33.737	2.64485	2.6546	501
36.538	36.545	2.45726	2.4567	431
44.627	44.633	2.02886	2.0285	700
47.025	47.052	1.9308	1.9297	711
48.694	48.721	1.86847	1.8675	004
50.533	50.492	1.80471	1.806	352
54.599	54.53	1.67952	1.6814	533
55.098	55.082	1.6655	1.6659	251
58.769	58.653	1.5699	1.5727	831
60.872	60.73	1.5206	1.5238	453

where  $h, k,$  and  $l$  are the Miller indices of the diffracting planes. These calculated values were found to be 1.4202, 1.159, and 0.7474 nm, for a, b, and c, respectively, with a unit cell volume of 123.0229 nm<sup>3</sup>, which are consistent with the standard diffraction pattern. The average crystallite size of the Sb<sub>2</sub>S<sub>3</sub> powder was calculated using the Gaussian fit of the main observed (022) plane according the well-known Scherrer's formula.

$$D = 0.9\lambda / \beta \cos\theta \quad (2)$$

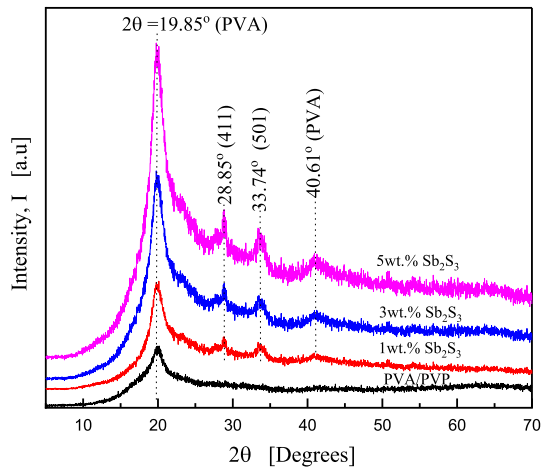
where  $D$  is the crystallite size,  $\lambda$  is the wavelength of the X-ray,  $\beta$  is full width at half maximum of the X-ray plane, and  $\theta$  is the diffraction angle. The calculated crystallite size using the Gaussian fit was found in a range of 24 nm. The transmission electron microscope and the corresponding histogram for the particle size determination are shown in Fig. 3a, b. The figure depicts a regular distribution for particles of the same shape. The TEM micrograph has been analyzed using ImageJ software to determine an average particle size of 40.66 nm. It was observed that there is a disagreement between the particle size calculated from both XRD and TEM. This can be attributed to the fact that XRD calculates the crystallite size while TEM determines the particle size which includes multiple crystallites (El-naggar et al. 2022a; El-Gamal and Sayed 2019).

Figure 4 illustrates the X-ray diffraction patterns of the prepared Sb<sub>2</sub>S<sub>3</sub>/PVA/PVP NPs polymeric sheets in the range of  $2\theta$  from 10 to 80. The figures exhibit a PVA/PVP characteristic broadening peak around  $2\theta = 19.5^\circ$ , attributed to the semi-crystalline nature of the PVA (Aziz et al. 2017a; Mohammed et al. 2018), and may be due to the presence of strong intra-molecular hydrogen bonding in isolated monomer units of PVA and inter-molecular hydrogen bonding between other monomer units (Mahendia et al. 2011). This characteristic peak is clearly also observed for all Sb<sub>2</sub>S<sub>3</sub>/PVA/PVP polymer sheets. Notably, there is also a slight peak observed at  $2\theta = 40.6^\circ$  for all Sb<sub>2</sub>S<sub>3</sub>/PVA/PVP curves which are related also to the semi-crystalline nature of PVA polymer (Aziz



**Fig. 3** **a** The transmission electron microscope and **b** the corresponding histogram for the particle size of the prepared  $\text{Sb}_2\text{S}_3$  NPs

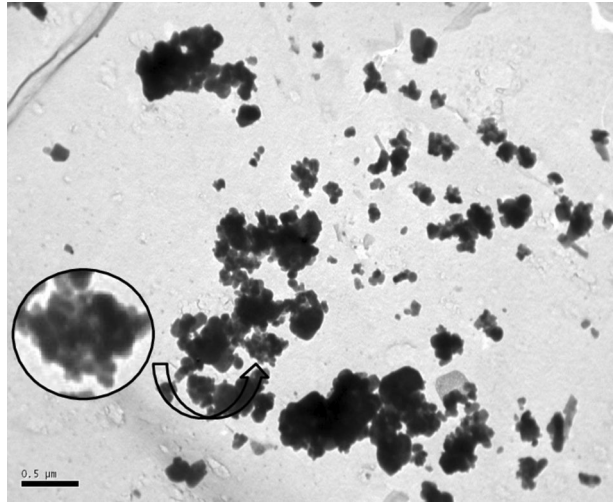
**Fig. 4** The X-ray diffraction patterns of the prepared  $\text{Sb}_2\text{S}_3$  NPs/PVA/PVP polymer sheet



et al. 2017a; Mohammed et al. 2018; Mahendia et al. 2011). The other peaks observed at  $2\theta = 28.53^\circ$ , and  $33.74^\circ$  correspond to  $\text{Sb}_2\text{S}_3$  peaks of (022), and (501), respectively.

Figure 5 represents the transmission electron micrograph of 5 wt.%  $\text{Sb}_2\text{S}_3$  NPs/PVA/PVP polymer sheet. It is observed that the high concentration of  $\text{Sb}_2\text{S}_3$  NPs aggregate in the PVA/PVP matrix, resulting in intermolecular and intramolecular hydrogen bonding of the polymer chains (Aziz 2016). So, as a result of the aggregation of NPs in a polymer matrix, an increase in the sample's crystallinity occurs as illustrated by XRD analysis. The inset of Fig. 5 represents the region that has been zoomed as assigned by the arrow where the grains of NPs are observed obviously.

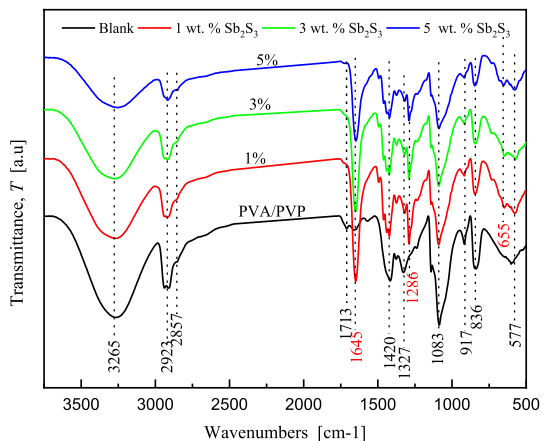
**Fig. 5** The transmission electron micrograph of 5 wt%  $\text{Sb}_2\text{S}_3$  NPs/PVA/PVP polymer sheet



### 3.2 FTIR analysis of pure PVA/PVP blend and $\text{Sb}_2\text{S}_3$ filled PVA/PVP polymeric nanocomposite sheets

Figure 6 shows the FTIR transmittance spectra of pure PVA/PVP polymer blend besides that doped with different doping weight ratios percentages (1, 3, and 5 wt%) of  $\text{Sb}_2\text{S}_3$  nanoparticles. The figure depicts the presence of a broad absorption peak centered at  $3283\text{ cm}^{-1}$  for pure PVA/PVP polymeric sheet, which corresponds to the O–H stretching vibration of hydroxyl groups of the PVA/PVP polymeric blend (Ali et al. 2018). The two bands observed at  $2857\text{ cm}^{-1}$  and  $2263\text{ cm}^{-1}$  were corresponding to C–H asymmetric stretching (Bhajantri et al. 2009; Abdullah et al. 2016), and C–H symmetric stretching (Zidan et al. 2019; Bhajantri et al. 2009). The band at  $1645\text{ cm}^{-1}$  is due to the C=O stretching of PVA and PVP (Zidan et al. 2016), thereby confirming the intermolecular interaction between the OH groups in PVA and carbonyl groups in PVP (Rajesh et al. 2019b; Gökmeşe et al. 2013). It was found that the intensity of this band increases as a result of adding the  $\text{Sb}_2\text{S}_3$

**Fig. 6** The FTIR transmittance spectra of pure PVA/PVP polymer sheet besides that doped with different doping weight ratios percentages (1, 3, and 5 wt%) of  $\text{Sb}_2\text{S}_3$  NPs



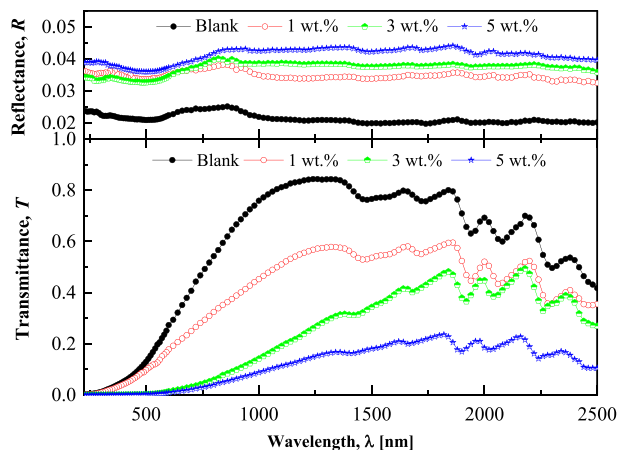


NPs powders to the PVA/PVP as a host matrix. The band at  $1420\text{ cm}^{-1}$  was assigned to the symmetric bending of  $\text{CH}_2$  vibration (Elashmawi et al. 2013). The band at  $1327\text{ cm}^{-1}$  in pure PVA/PVP was shifted to  $1286\text{ cm}^{-1}$  due to the S–S vibration in nanoparticles of  $\text{Sb}_2\text{S}_3$  structure and enhanced after PVA/PVP polymeric was melded with  $\text{Sb}_2\text{S}_3$  NPs powders. The observed increase of the band at  $1645\text{ cm}^{-1}$  besides the shift of the band from  $1327$  to  $1286\text{ cm}^{-1}$ , reflects the success of the interaction between the filler  $\text{Sb}_2\text{S}_3$  material with the PVA/PVP as a host polymeric matrix. The bands at 1083 and 917 were attributed, respectively, to C=O stretching (Zidan et al. 2019), and  $\text{CH}_2$  rocking (Abdelghany et al. 2016). Other bands at 836 and 577, were attributed respectively, to C–C stretching (Om-karam et al. 2007) and N–C=O bending vibrations (Safo et al. 2019; Kamaruddin et al. 2017; Rezeki et al. 2019; Bryaskova et al. 2011). The FTIR spectra show also a weak absorption band observed at  $655\text{ cm}^{-1}$  which is related to the stretching vibration of Sb-S.

### 3.3 Optical properties

Figure 7 illustrates the optical transmittance and reflectance spectra of  $\text{Sb}_2\text{S}_3$ /PVA/PVP NPs polymer sheets in the wavelength range 250–2500 nm. The figure depicts that a pure PVA/PVP sheet exhibits high transparency reaching a value of 82% which agrees quite well with that reported previously (Badawi 2020). The transmittance spectra of  $\text{Sb}_2\text{S}_3$ /PVA/PVP NPs polymer sheets showed a drastic decrease with increasing  $\text{Sb}_2\text{S}_3$  wt%. The transmittance spectra of the samples can be divided into two different regions. The 1st region is related to the fundamental absorption region in the optical wavelength range 250–1000 nm at which the polymer sheets strongly and gradually absorb the incident radiation. It was observed that the fundamental absorption edge of the pure PVA/PVP and those filled with 1 and 3 wt%  $\text{Sb}_2\text{S}_3$  NPs shift to a higher wavelength side (red-shift). However, with the increase of the filling  $\text{Sb}_2\text{S}_3$  NPs concentration in the PVA/PVP matrix to 5 wt%, the fundamental absorption edge shifts to the shorter wavelength (blue shift), reflecting a variation of the optical band gap in a reverse manner. These variations reflect an active incorporation of the filled  $\text{Sb}_2\text{S}_3$  NPs in the PVA/PVP host matrix. The variation of the optical band gap energy against the variation of the  $\text{Sb}_2\text{S}_3$  NPs filling percent in the PVA/PVP matrix will be illustrated below. The 2nd region within the wavelength range 1450–2320 nm, in which the transmission spectra contain five multi-oscillations absorption bands located, respectively, at 1482, 1746, 1958, 2100, and

**Fig. 7** The optical transmission and reflection spectra of the  $\text{Sb}_2\text{S}_3$ /PVA/PVP polymer sheets



2320 nm, which are related to the first overtone of the -CH group (Sultanova et al. 2012). Similar behavior of the transmission spectra was reported elsewhere (Badawi 2020; AlAbdulaal et al. 2022). It was also observed that the reflectance spectra of the investigated samples increase with increasing the embedded Sb<sub>2</sub>S<sub>3</sub> NPs in the PVA/PVP host matrix in a reverse manner to the behavior of the transmittance spectra. The optical constants (real and imaginary parts of the refractive index, n, and k) were calculated as functions of the incident wavelength from the recorded transmittance and reflectance spectra via the relations (Mohammed et al. 2018; Subramanian and C.I. P, P.P. D, 2010):

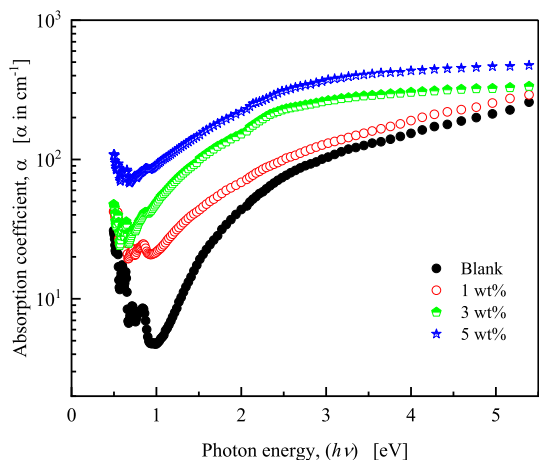
$$\alpha = \left(\frac{1}{d}\right) \ln\left(\frac{(1-R)^2}{T}\right) \text{cm}^{-1} \tag{3}$$

$$n = \left\{ \sqrt{\frac{4R}{(1-R)^2} - k^2} + \frac{(1+R)}{(1-R)} \right\} \tag{4}$$

where  $\alpha$  is the absorption coefficient ( $\alpha = 4\pi k/\lambda$ ),  $d$  is the sheet thickness,  $T$  is the transmittance,  $R$  is the reflectance and  $\lambda$  is the wavelength of the incidence wavelength. The Spectral variations of the absorption coefficient,  $\alpha$  as a function of the photon energy, ( $h\nu$ ) using Eq. 3 are shown in Fig. 8. The figure depicts an exponential dependence of the absorption coefficient on the photon energy. At lower energy <2 eV, the absorption coefficient is slightly low, this may be attributed to the fact that the energy of the incident photon energy is not sufficient to transmit the electrons from the valence band to the conduction band. While at higher energies, the incident photon energy is sufficient to free electrons to high levels, which reflects an increase in the absorption coefficient. On the other hand, the absorption coefficient of nanocomposite polymer sheets increases with increasing concentrations of the NPs Sb<sub>2</sub>S<sub>3</sub> wt% in the PVA/PVP host matrix which reflects increases in the number of charge carriers. The absorption coefficient in the fundamental absorption region can be described by Tauc's relation (Mohammed et al. 2018):

$$(\alpha h\nu) = B(h\nu - E_g)^n \tag{5}$$

**Fig. 8** The spectral variation of the absorption coefficient,  $\alpha$ , as a function of the phone energy for the Sb<sub>2</sub>S<sub>3</sub>/PVA/PVP polymer sheets



where  $B$  is a constant and  $n$  is an exponent characterizing the nature of the optical transition process in the  $k$ -space causing the optical absorption. Plots  $(\alpha h\nu)^2$  vs.  $(h\nu)$  for a direct optical transition as shown in Fig. 9, and extrapolating the linear part of the curves to zero energy one can estimate the values of the energy band gap, which are listed in Table 2. The value of the optical band gap energy for pure PVA/PVP sheet is 4.68 eV in context with the values of 4.95 eV, for PVA/PVP blended with the ratio 50/50 (Badawi 2020), with the value of 4.66 eV for 40/60 PVA/PVP (El-Mahalawy et al. 2023), 4.88 eV for 50/50 PVA/PVP (El-naggar et al. 2021), 5.26 eV for 70/30 PVA/PVP (El-naggar et al. 2022a), and 4.97 eV for 70/30 PVA/PVP (Heiba et al. 2021b). The value of the energy band gap decreases from 4.68 eV for pure PVA/PVP to the value of 4.21 and 3.03 eV, respectively, due to increasing  $\text{Sb}_2\text{S}_3$  NPs filling in the PVA/PVP blend matrix to 1%, and 3 wt%, respectively. This decrease in the  $E_g$  value can be attributed to an increase in the degree of the disordered of the PVA/PVP blend matrix due to filling with  $\text{Sb}_2\text{S}_3$  NPs (Abdullah et al. 2016, 2015b), hence creating a localized state in the band gap as a result of  $\text{Sb}_2\text{S}_3$  doping. However, the determined band gap value in the case of the PVA/PVP sheet filled with 5% increased as the opposite of expected to 3.19 eV rather than a decrease as in the two other cases. The results of the optical band gap of the  $\text{Sb}_2\text{S}_3$ /PVA/PVP polymer sheets make them effective candidates for optoelectronics applications and optical devices. For instance, 5 wt% of  $\text{Sb}_2\text{S}_3$ -filled PVA/PVP polymer blend sheet which possesses a band gap of 3.19 eV, corresponding to  $\lambda \approx 389$  nm, could be used as an effective UV blocker filter (Badawi 2020).

The variation of the optical band gap energy could be also calculated as a result of doping  $\text{Sb}_2\text{S}_3$  NPs wt% in the PVA/PVP host matrix, using the absorption spectra of the investigated samples shown in Fig. 10a, based on the absorption spectrum fitting model (ASF). According to this model, the absorption coefficient in Eq. (5) can be expressed as a function of wavelength by El-Mahalawy et al. (2023); Nasrallah and Ibrahim 2022; Bhogi et al. 2022):

$$\alpha(\lambda) = B(hc)^{n-1} \lambda \left( \frac{1}{\lambda} - \frac{1}{\lambda_g} \right)^n \quad (6)$$

where  $\lambda_g$ ,  $h$  and  $c$  are the wavelength conformable to the optical band gap, plank's constant and velocity of light, respectively. The Eq. (6) will be rewritten on the basis of Beer-Lambert's law as follows:

**Fig. 9** Plots of  $(\alpha h\nu)^2$  vs.  $(h\nu)$  for pure PVA/PVP and  $\text{Sb}_2\text{S}_3$ /PVA/PVP polymer sheets

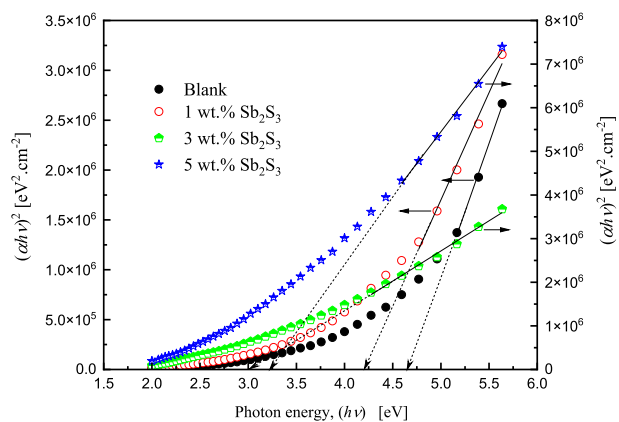


**Table 2** The optical parameters of pure PVA/PVP and Sb<sub>2</sub>S<sub>3</sub>/PVA/PVP

Sample state	$E_g^{(0020)}$ [eV]	$E_g^{ASFT}$ [eV]	$E_d$ [eV]	$E_o$ [eV]	$n_o$	$E_g^{WDP}$ [eV]	$f = E_o E_d [eV]^2$	$\epsilon_s$	$\epsilon_L$	$N/m^*$ (Kg <sup>-1</sup> m <sup>-3</sup> )
Blank	4.68	4.29	7.14	9.28	1.33	4.64	47.96	1.77	1.78	$1.93 \times 10^{54}$
1 wt% Sb <sub>2</sub> S <sub>3</sub>	4.21	4.09	9.48	8.57	1.45	4.29	71.38	2.11	2.13	$5.65 \times 10^{54}$
3 wt% Sb <sub>2</sub> S <sub>3</sub>	3.03	2.91	7.05	5.98	1.48	2.99	38.23	2.18	2.22	$7.90 \times 10^{54}$
5 wt% Sb <sub>2</sub> S <sub>3</sub>	3.19	3.14	8.32	6.43	1.50	3.21	15.95	2.30	2.36	$2.19 \times 10^{55}$

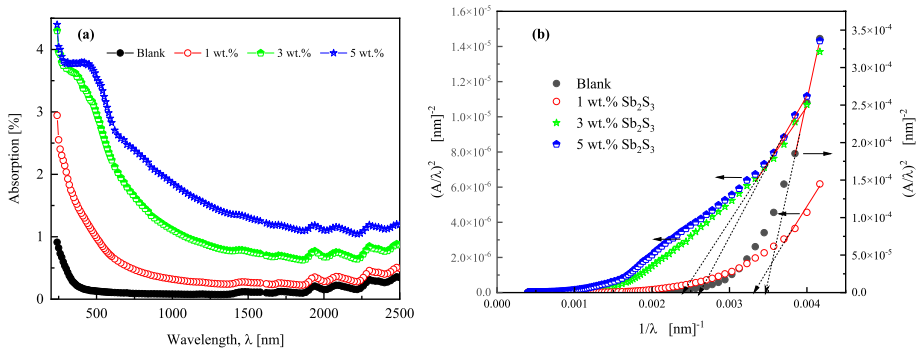


**Fig. 10** **a** The optical absorbance spectra, and **b** Plots  $(A/\lambda)^2$  vs.  $(1/\lambda)$  for pure PVA/PVP and  $Sb_2S_3$ /PVA/PVP polymer sheets

$$A(\lambda) = D_1 \lambda \left( \frac{1}{\lambda} - \frac{1}{\lambda_g} \right)^n + D_2 \quad (7)$$

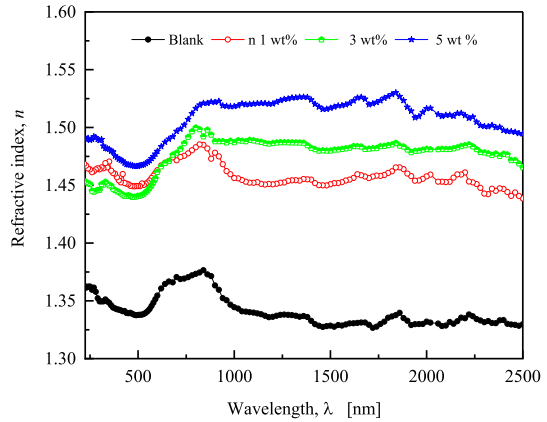
where  $D_1 = (B(hc)^{n-1}d/2.303)$  and  $D_2$  is a constant that is considered to be a reflection. For the direct optical transition, the extrapolation of the linear part in  $(A/\lambda)^2$  vs.  $(1/\lambda)$  plot as shown in Fig. 10b provides the value of  $1/\lambda_g$ , which can then be used to determine the optical band gap as follows:

$$E_g^{ASF} = \frac{1239.83}{\lambda_g} \quad (8)$$

The calculated  $E_g^{ASF}$  values for the investigated samples are listed in Table 2. It can be noticed that the values of  $E_g^{ASF}$  agree very well with the  $E_g^d$  values calculated using Tauc's relation and have the same trend. As the doping content of  $Sb_2S_3$  NPs increases in the PVA/PVP blend up to 3 wt%, the energy gap reduces. However, for the PVA/PVP blend filled with 5 wt%  $Sb_2S_3$  NPs, the energy gap increases. The increase in the optical band energy of the PVA/PVP sample filled with 5  $Sb_2S_3$  wt% can be interpreted as the following. At low concentrations of  $Sb_2S_3$  NPs, the grains of NPs are randomly and uniformly distributed throughout the PVA/PVP matrix (Dissanayake et al. 2003). The presence of these grains can create additional favorable conducting pathways near their surface, where the number of them increases with increasing surface area of NPs added to the PVA/PVP matrix. Therefore, the charge carriers can transfer between these conducting pathways leading to an increase in the conduction and, consequently a decrease in the optical band gap. Further increase of  $Sb_2S_3$  NPs may result in the aggregation of the NPs in the PVA/PVP matrix, which leads to the immobilization of longer polymer chains (El-Gamal and Sayed 2019; Dissanayake et al. 2003; Aziz et al. 2017b). This, in turn, reduces the surface area of the NPs, causing a decrease in the conduction and, consequently an increase in the optical band gap. The aggregation of the grains has been confirmed earlier by TEM.

The spectral variations of the refractive index,  $n$  against the wavelength for pure PVA/PVP and PVA/PVP polymeric sheets filled with different wt% of  $Sb_2S_3$  NPs are shown in Fig. 11. The figure depicts that the investigated samples exhibit a peak occurring for all samples observed in the wavelength range 500 and 850 nm, which may be due to the electronic transition from bonding to antibonding molecular orbital (Elrasasi et al. 2022). The refractive index variation vs. wavelength for each of the investigated samples shows

**Fig. 11** The spectral variation of the refractive index,  $n$  against the wavelength for pure PVA/PVP and different wt% of  $Sb_2S_3$  blending with PVA/PVP polymer sheets



un-systematic behavior within the wavelength range 800–1850 nm (slightly up and down) which may be attributed to the presence of some of the absorption bands in the transmission and/or reflection spectra, while beyond 1850 nm, it begins to decrease gradually with the wavelength. Whereas, beyond the wavelength 850 nm, the refractive index notably increases with increasing the addition of  $Sb_2S_3$  content into the PVA/PVP as a host matrix. This implies that the density of the PVA/PVP melded polymer increased with an increase in the amount of  $Sb_2S_3$  wt% (Muhammad et al. 2015).

The refractive index can be analyzed according to Wemple DiDomenico single oscillator model (Wemple and DiDomenico 1971; Teleb et al. 2021). According to the model, the refractive index  $n$  is related to the oscillator energy,  $E_o$ , and the dispersion energy  $E_d$  via relations:

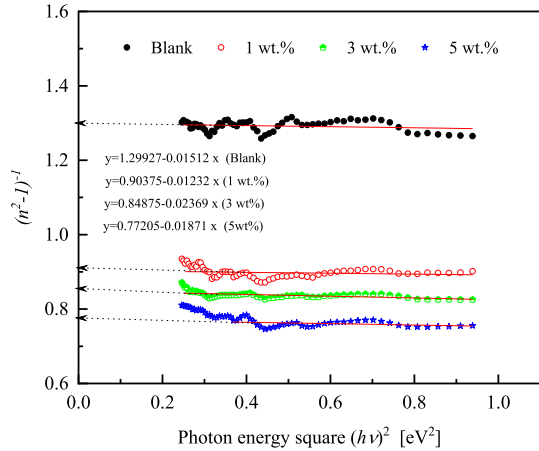
$$(n^2 - 1) = \frac{E_d E_o}{E_o^2 - (hv)^2} \tag{9}$$

*i.e.*

$$(n^2 - 1)^{-1} = \frac{E_o}{E_d} - \left( \frac{1}{E_o E_d} \right) (hv)^2 \tag{10}$$

where  $hv$  is the photon energy. Experimental fulfillment of this relation can be obtained by plotting  $(n^2 - 1)^{-1}$  vs.  $(hv)^2$  in the photon energy range 0.24–0.94 eV<sup>2</sup> as shown in Fig. 12, for natural behavior. Linear fits of the function to the smaller energy data yield straight lines equations as shown in Fig. 12 allowing us to determine the values of  $(E_o E_d)^{-1}$  and  $(E_d/E_d)$  from the slope and intercept, respectively. The determined oscillator parameters values  $E_o$ ,  $E_d$ , the static refractive index,  $n_o^2 = (1 + E_d/E_o)$  where  $n_o(0) = nathv \rightarrow 0$ , the oscillator strength  $f$ , ( $f = E_o E_d$ ) as well as the value of the static high-frequency dielectric constant  $\epsilon_s = n_s^2$  are listed in Table 2. It was seen from the listed data that the trend of variation in the oscillator energy values,  $E_o$  calculated from the Wemple DiDomenico model follows the same variation trend of the calculated optical band gap values for each of the Tauc’s or ASF models, which indicates the applicability of the applied Wemple DiDomenico model in this work. Where the values of the single oscillator energy,  $E_o$ , decrease from 4.04 to 3.15 eV, and dispersion energy,  $E_d$  decreases from 3.77 to 3.55 eV, as the  $Sb_2S_3$  NPs filler increases in the PVA/PVP polymer matrix from 1 to 3 wt%.

**Fig. 12** Plots of  $(n^2 - 1)^{-1}$  vs.  $h\nu^2$  for pure PVA/PVP and  $\text{Sb}_2\text{S}_3$ /PVA/PVP polymer sheets. The inset shows the fitting equation for each sample



Further analysis of the refractive index data at long wavelength region (1500 – 2500nm) was also performed on the basis of the Drude free electron model to elucidate the effects of filling  $\text{Sb}_2\text{S}_3$  NPs to the PVA/PVP as a host matrix on the variation the carrier concentration to the effective mass ratio,  $N/m^*$  as well as the lattice high dielectric constant,  $\epsilon_\infty$  using the relations (Ammar et al. 2015; El-Gendy 2017):

$$\epsilon_r = n^2 - k^2 = \epsilon_L - \left(\frac{e^2}{4\pi\epsilon_0 c^2}\right)\left(\frac{N}{m^*}\right)\lambda^2 \quad (11)$$

where  $e$  is the electron charge,  $\epsilon_0$  the permittivity of the free space ( $= 8.854 \times 10^{-12}$  F/m),  $\epsilon_\infty$  the high lattice dielectric constant, and  $N/m^*$  is the carrier concentration to the effective mass ratio. The values of  $N/m^*$  as well as the lattice high-frequency dielectric constant,  $\epsilon_\infty$  could be determined, respectively, from the slope and intercept of the plots  $\epsilon_r$  vs.  $\lambda^2$  shown in Fig. 13. Those values are listed in Table 2. It is evident from those values that, for all of the investigated samples  $\epsilon_L > \epsilon_s$  which are mainly attributed to the contribution of the free carriers-concentration to the lattice vibration in the dispersion modes (El-Gendy 2017; Qasrawi and Shukri Ahmad 2006). It was noticed that the calculated  $N/m^*$  values increase with the increasing addition of  $\text{Sb}_2\text{S}_3$  in the polymeric mixture, which indicates an increase in charge carriers.

The optical conductivity is related to the absorption coefficient and the refractive index of the prepared samples by the relation (Abdullah et al. 2016; Abd El-Ghany et al. 2022):

$$\sigma = \frac{\alpha n c}{4\pi} \quad (12)$$

where  $\alpha$  is absorption coefficient,  $n$  is the refractive index and  $c$  is the light speed. Figure 14 shows the variation of optical conductivity with photon energy. Obviously, the optical conductivity increases with the addition of  $\text{Sb}_2\text{S}_3$ . This means that the concentration of charge carriers increases in the PVA/PVP matrix due to the dispersion of  $\text{Sb}_2\text{S}_3$  in the interstitial spaces of the polymer chains (Badawi 2020; Abdullah et al. 2015b). Additionally, the increase in the optical conductivity at the high photon energy is due to the high absorption of ultraviolet radiation by the prepared samples (Abdullah et al. 2016).

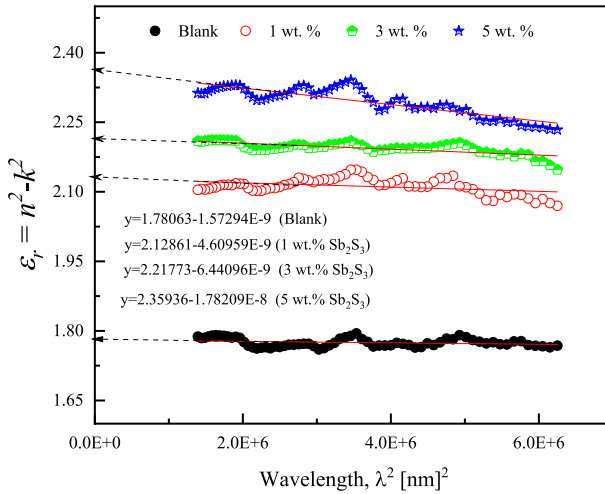


**Fig. 13** Plots of  $\epsilon_r$  vs.  $\lambda^2$  for pure PVA/PVP and  $\text{Sb}_2\text{S}_3$ /PVA/PVP polymer sheets. The inset shows the fitting equation for each sample

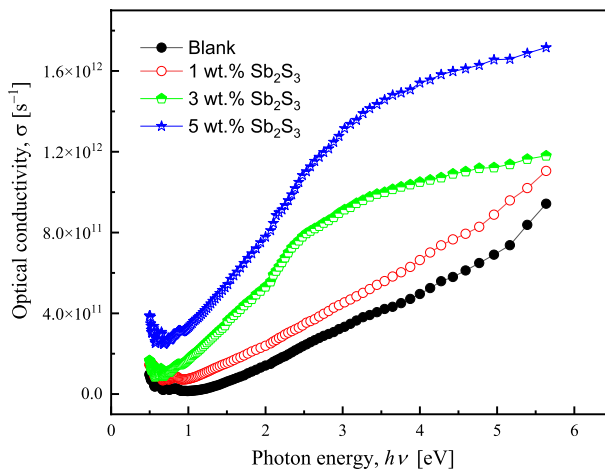


**Fig. 14** Plots of  $\sigma$  vs.  $h\nu$  for pure PVA/PVP and  $\text{Sb}_2\text{S}_3$ /PVA/PVP polymer sheets

## 4 Conclusions

The chemical co-precipitation method has been used at low temperatures to prepare the  $\text{Sb}_2\text{S}_3$  powder sample. The X-ray diffraction studies of the powder revealed that the X-ray diffraction pattern exhibits a polycrystalline orthorhombic structure of crystallite size of 24 nm. Different ratios of 0, 1, 3, and 5 wt% of  $\text{Sb}_2\text{S}_3$  were filled with the PVA/PVP (2:1) polymer sheets via the solution cast technique. The FT-IR spectra indicate an effective incorporation of the  $\text{Sb}_2\text{S}_3$  filled in the PVA/PVP host matrix. The optical band gap energy for PVA/PVP samples filled with 1% and 3 wt%  $\text{Sb}_2\text{S}_3$  NPs show at first decreases from



4.68 to 3.03 eV and thereafter increases further to 3.19 eV for the sample filled with 5 wt%  $\text{Sb}_2\text{S}_3$  NPs. The refractive index-dispersion analysis is adequately described by the single oscillator model. The single oscillator energy,  $E_o$  decreases from 9.28 to 5.98 eV as the PVA/PVP host matrix is filled with  $\text{Sb}_2\text{S}_3$  NPs of 1 and 3 wt%, while the filler content increases to 5 wt%,  $E_o$  then increases to 6.43 eV. The carrier concentration to the effective mass ratio was also evaluated as a function of filling  $\text{Sb}_2\text{S}_3$  wt%. It is worth noting here to point out that, the large variation in the optical properties of PVA/PVP blended sheets filled with  $\text{Sb}_2\text{S}_3$  makes them effective candidates for optoelectronic and optical applications.

**Author contributions** N.M. Farrage: Prepared the samples, performed the IR analysis, and wrote the original draft. Nahed H. Teleb: Performed the x-ray analysis and TEM analysis and wrote the original draft. W.A. Abd El-Ghany: Performed the optical analysis and review & editing.

**Funding** Open access funding provided by The Science, Technology & Innovation Funding Authority (STDF) in cooperation with The Egyptian Knowledge Bank (EKB). The authors haven't any funds for this publication.

## Declarations

**Conflict of interest** The authors declare that they have no known competing financial interests or personal relationships that could have appeared to influence the work reported in this paper.

**Open Access** This article is licensed under a Creative Commons Attribution 4.0 International License, which permits use, sharing, adaptation, distribution and reproduction in any medium or format, as long as you give appropriate credit to the original author(s) and the source, provide a link to the Creative Commons licence, and indicate if changes were made. The images or other third party material in this article are included in the article's Creative Commons licence, unless indicated otherwise in a credit line to the material. If material is not included in the article's Creative Commons licence and your intended use is not permitted by statutory regulation or exceeds the permitted use, you will need to obtain permission directly from the copyright holder. To view a copy of this licence, visit <http://creativecommons.org/licenses/by/4.0/>.

## References

- Abd El-Ghany, W.A., Nasralla, N.H.S., El Komy, G.M.: Structure and optical properties of spray deposited Cu–Mn–O thin films for optoelectronic devices. *Opt. Mater.* **127**, 112319 (2022)
- Abd El-Kader, M.F.H., Elabbasy, M.T., Adeboye, A.A., Menazea, A.A.: Nanocomposite of PVA/PVP blend incorporated by copper oxide nanoparticles via nanosecond laser ablation for antibacterial activity enhancement. *Polym. Bull.* **79**, 9779–9795 (2021)
- Abdelghany, A.M., Abdelrazek, E.M., Tarabiah, A.E.: Modeling and physical properties of lead sulphide/polyvinyl alcohol nano-composite. *Quant. Matt.* **5**, 257–262 (2016)
- Abdelrazek, E.M., Elashmawi, I.S., El-khodary, A., Yassin, A.: Structural, optical, thermal and electrical studies on PVA/PVP blends filled with lithium bromide. *Curr. Appl. Phys.* **10**, 607–613 (2010)
- Abdullah, O.G., Tahir, D.A., Kadir, K.: Optical and structural investigation of synthesized PVA/PbS nanocomposites. *J. Mater. Sci. Mater. Electron.* **26**, 6939–6944 (2015a)
- Abdullah, O.G., Aziz, S.B., Omer, K.M., Salih, Y.M.: Reducing the optical band gap of polyvinyl alcohol (PVA) based nanocomposite. *J. Mater. Sci. Mater. Electron.* **26**, 5303–5309 (2015b)
- Abdullah, O.G., Aziz, S.B., Rasheed, M.A.: Structural and optical characterization of PVA:KMnO<sub>4</sub> based solid polymer electrolyte. *Results Phys.* **6**, 1103–1108 (2016)
- AlAbdulaal, T.H., Almoadi, A., Yahia, I.S., Zahra, H.Y., Alqahtani, M.S., Yousef, E.S., Hussein, K.I., Jalah, M., Harraz, F.A., Al-Assiri, M.S.: High optical performance of Gd<sub>2</sub>O<sub>3</sub>-doped PVA/PVP composite films for electronic and laser CUT-OFF filters. *Optik* **268**, 169741 (2022)
- Ali, F.M., Kersh, R.M., Sayed, M.A., AbouDeif, Y.M.: Evaluation of structural and optical properties of Ce<sup>3+</sup> ions doped (PVA/PVP) composite films for new organic semiconductors. *Phys. B* **538**, 160–166 (2018)

- Al-Ramadhan, Z.A., Salman, J.A., Hmud, H.A.K.: Optical and morphological properties of (PVA-PVP-Ag) nanocomposites. *Int. J. Sci. Res.* **5**, 1828–1836 (2016)
- Alsaad, A., Al Dairy, A.R., Ahmad, A., Qattan, I.A., Al Fawares, S., Al-Bataineh, Q.: Synthesis and characterization of polymeric (PMMA-PVA) hybrid thin films doped with TiO<sub>2</sub> nanoparticles using dip-coating technique. *Crystals* **11**, 99 (2021)
- Ammar, A.H., Farid, A.M., Farag, A.A.M., Sharshar, K.A.A., Abu-Samaha, F.S.H., Hamad, K.M.: Structural, absorption, dispersion and photo-induced characteristics of thermally vacuum-evaporated BiSbSe<sub>3</sub> thin films. *J. Non-Cryst. Solids* **416**, 50–57 (2015)
- Arumugam, J., Raj, A.D., Irudayaraj, A.A., Thambidurai, M.: Solvothermal synthesis of Bi<sub>2</sub>S<sub>3</sub> nanoparticles and nanorods towards solar cell application. *Mater. Lett.* **220**, 28–31 (2018a)
- Arumugam, J., Raj, A.D., Irudayaraj, A.A.: Reaction time dependent investigation on the properties of the Bi<sub>2</sub>S<sub>3</sub> nanoparticles: photocatalytic application. *Mater. Today Proc.* **5**, 16094–16099 (2018b)
- Aziz, S.B.: Role of dielectric constant on ion transport: reformulated arrhenius equation. *Adv. Mater. Sci. Eng.* **2016**, 1–11 (2016)
- Aziz, S.B., Rasheed, M.A., Abidin, Z.H.Z.: Optical and electrical characteristics of silver ion conducting nanocomposite solid polymer electrolytes based on chitosan. *J. Electron. Mater.* **46**, 6119–6130 (2017b)
- Aziz, S.B., Rasheed, M.A., Hussein, A.M., Ahmed, H.M.: Fabrication of polymer blend composites based on [PVA-PVP]<sub>(1-x)</sub>:(Ag<sub>2</sub>S)<sub>x</sub> (0.01 ≤ x ≤ 0.03) with small optical band gaps: structural and optical properties. *Mater. Sci. Semicond. Proc.* **71**, 197–203 (2017a)
- Badawi, A.: Engineering the optical properties of PVA/PVP polymeric blend in situ using tin sulfide for optoelectronics. *Appl. Phys. A* **126**, 335 (2020)
- Badawi, A.: Enhancement of the optical properties of PVP using Zn<sub>1-x</sub>Sn<sub>x</sub>S for UV-region optical applications. *Appl. Phys. A* **127**, 51 (2021)
- Baraker, B.M., Lobo, B.: Experimental study of PVA-PVP blend films doped with cadmium chloride monohydrate. *Indian J. Pure Appl. Phys.* **54**, 634–640 (2016)
- Bdewi, S.F., Abdullah, O.G., Aziz, B.K., Mutar, A.A.R.: Synthesis, structural and optical characterization of MgO nanocrystalline embedded in PVA matrix. *J. Inorg. Organomet. Polym. Mater.* **26**, 326–334 (2016)
- Ben Doudou, B., Vivet, A., Chen, J., Laachachi, A., Falher, T., Poilâne, C.: Hybrid carbon nanotube—silica/ polyvinyl alcohol nanocomposites films: preparation and characterisation. *J. Polym. Res.* **21**, 1–9 (2014)
- Bhajantri, R.F., Ravindrachary, V., Poojary, B., Ismayil, A., Harisha, V., Crasta, P.T.: Studies on fluorescent PVA + PVP + MPDMAPP composite films. *Polym. Eng. Sci.* **49**, 903–909 (2009)
- Bhogi, A., Srinivas, B., Padmavathi, P., Venkataramana, K., Ganta, K.K., Shareefuddin, M., Kistaiah, P.: Absorption spectrum fitting method (ASF), DASF method and structural studies of Li<sub>2</sub>O–SrO–B<sub>2</sub>O<sub>3</sub>–MnO quaternary glass system. *Opt. Mater.* **133**, 112911 (2022)
- Bryaskova, R., Pencheva, D., Nikolov, S., Kantardjiev, T.: Synthesis and comparative study on the antimicrobial activity of hybrid materials based on silver nanoparticles (AgNps) stabilized by polyvinylpyrrolidone (PVP). *J. Chem. Biol.* **4**, 185–191 (2011)
- Cullity, B.D.: Elements of X-Ray Diffraction, 2nd edn. Addison-Wesley Publishing Company, Boston (1978)
- Dissanayake, M.A.K.L., Jayathilaka, P.A.R.D., Bokalawala, R.S.P., Albinsson, I., Mellander, B.E.: Effect of concentration and grain size of alumina filler on the ionic conductivity enhancement of the (PEO)<sub>9</sub>LiCF<sub>3</sub>SO<sub>3</sub>:Al<sub>2</sub>O<sub>3</sub> composite polymer electrolyte. *J. Power. Sources* **119–121**, 409–414 (2003)
- El Fewaty, N.H., El Sayed, A.M., Hafez, R.S.: Synthesis, structural and optical properties of tin oxide nanoparticles and its CMC/PEG–PVA nanocomposite films. *Polym. Sci., Ser. A* **58**, 1004–1016 (2016)
- Elashmawi, I.S., Abdelghany, A.M., Hakeem, N.A.: Quantum confinement effect of CdS nanoparticles dispersed within PVP/PVA nanocomposites. *J. Mater. Sci. Mater. Electron.* **24**, 2956–2961 (2013)
- Elashmawi, I., Abdelrazek, E., Yassin, A.: Influence of NiCl<sub>2</sub>/CdCl<sub>2</sub> as mixed filler on structural, thermal and electrical properties of PVA/PVP blend, *British. J. Appl. Sci. Technol.* **4**, 4263–4279 (2014)
- Elashmawi, I.S., Abdel Baieth, H.E.: Spectroscopic studies of hydroxyapatite in PVP/PVA polymeric matrix as biomaterial. *Curr. Appl. Phys.* **2**, 141–146 (2012)
- El-Gamal, S., El Sayed, A.M.: Physical properties of the organic polymeric blend (PVA/PAM) modified with MgO nanofillers. *J. Compos. Mater.* **53**, 2831–2847 (2019)
- El-Gendy, Y.A.: Effects of film thickness on the linear and nonlinear refractive index of p-type SnO films deposited by e-beam evaporation process. *Physica B* **526**, 59–63 (2017)
- El-Mahalawy, A.M., Abdrabou, M.M., Mansour, S.A., Ali, F.M.: Appreciably optimization of PVA/PVP nanocomposite blend for enhanced optoelectronics properties and multifunctional applications. *Physica B* **650**, 414586 (2023)

- El-naggar, A.M., Heiba, Z.K., Mohamed, M.B., Kamal, A.M., Osman, M.M., Albassam, A.A., Lakshminarayana, G.: Improvement of the optical characteristics of PVA/PVP blend with different concentrations of SnS<sub>2</sub>/Fe. *J. Vinyl Addit. Technol.* **28**, 82–93 (2022a)
- El-naggar, A.M., Heiba, Z.K., Mohamed, M.B., Kamal, A.M., Abd-Elkader, O.H., Lakshminarayana, G.: Effect of ZnO/(Co or Mn) ratios on the structure and optical spectroscopy parameters of PVA/PVP/PEG blended polymer. *Opt. Mater.* **128**, 112411 (2022b)
- El-naggar, A.M., Heiba, Z.K., Mohamed, M.B., Kamal, A.M., Osman, M.M., Albassam, A.A., Lakshminarayana, G.: Embedding of 50%PVA/50%PVP blend with Sn<sub>0.75</sub>M<sub>0.25</sub>S<sub>2</sub>, (M = Y, Fe, Cr, V); structural and optical study. *Appl. Phys. A* **127**, 753 (2021)
- Elrasasi, T.Y., Attallah, M.A., Shash, N.M., El-Shaarawy, M.G.: Linear and non-linear optical properties of PVA–Ag/Coumarin Nanocomposites. *Egypt J. Solids* **44**, 1–25 (2022)
- Gökmeşe, F., Uslu, İ, Aytimur, A.: Preparation and characterization of PVA/PVP nanofibers as promising materials for wound dressing. *Polym.-Plast. Technol. Eng.* **52**, 1259–1265 (2013)
- Hatta, F.F., Yahya, M.Z.A., Ali, A.M.M., Subban, R.H.Y., Harun, M.K., Mohamad, A.A.: Electrical conductivity studies on PVA/PVP-KOH alkaline solid polymer blend electrolyte. *Ionics* **11**, 418–422 (2005)
- Heiba, Z.K., Mohamed, M.B.: Effect of annealed and Mg-doped nano ZnO on physical properties of PVA. *J. Mol. Struct.* **1181**, 507–517 (2019)
- Heiba, Z.K., Mohamed, M.B., Imam, N.G.: Fine-tune optical absorption and light emitting behavior of the CdS/PVA hybridized film nanocomposite. *J. Mol. Struct.* **1136**, 321–329 (2017)
- Heiba, Z.K., Mohamed, M.B., Badawi, A., Alhazime, A.A.: The role of Cd<sub>0.9</sub>Mg<sub>0.1</sub>S nanofillers on the structural, optical, and dielectric properties of PVA/CMC polymeric blend. *Chem. Phys. Lett.* **770**, 138460 (2021a)
- Heiba, Z.K., El-naggar, A.M., Mohamed, M.B., Altowairqi, Y., Kamal, A.M.: Noval properties of PVA/PVP polymer blend doped by nano-ZnO/M (M = Co, Cu, Mn, V). *Appl. Phys. A* **127**, 976 (2021b)
- Heiba, Z.K., Bakr Mohamed, M., Ahmed, S.I.: Exploring the physical properties of PVA/PEG polymeric material upon doping with nano gadolinium oxide. *Alex. Eng. J.* **61**, 3375–3383 (2022)
- Helberg, R.M.L., Dai, Z., Ansaloni, L., Deng, L.: PVA/PVP blend polymer matrix for hosting carriers in facilitated transport membranes: synergistic enhancement of CO<sub>2</sub> separation performance, *Green. Energy Environ.* **5**, 59–68 (2020)
- Hemalatha, K.S., Rukmani, K., Suriyamurthy, N., Nagabushana, B.M.: Synthesis, characterization and optical properties of hybrid PVA–ZnO nanocomposite: a composition dependent study. *Mater. Res. Bull.* **51**, 438–446 (2014)
- Kamaruddin, D., Edikresna, I., Sriyanti, M.M.: Munir, khairurrijal, synthesis of polyvinylpyrrolidone (PVP)-green tea extract composite nanostructures using electrohydrodynamic spraying technique. *IOP Conf. Ser. Mater. Sci. Eng.* **202**, 012043 (2017)
- Kochi, R., Crasta, V., Kumar, R., Shetty, G.: Study of structural, optical and photoluminescence properties of ZnO doped PVA/PVP nanocomposite. *AIP Conf. Proc.* **2100**, 020045 (2019)
- Li, Y., Zhu, C., Fan, D., Fu, R., Ma, P., Duan, Z., Li, X., Lei, H., Chi, L.: Construction of porous sponge-like PVA-CMC-PEG hydrogels with pH-sensitivity via phase separation for wound dressing, *international journal of polymeric materials and polymeric.* *Biomaterials* **69**, 505–515 (2019)
- Mahendia, S., Tomar, A.K., Chahal, R.P., Goyal, P., Kumar, S.: Optical and structural properties of poly(vinyl alcohol) films embedded with citrate-stabilized gold nanoparticles. *J. Phys. D Appl. Phys.* **44**, 205105 (2011)
- Mohamed, M.B., Heiba, Z.K., Imam, N.G.: Optical and thermogravimetric analysis of Zn<sub>1-x</sub>Cu<sub>x</sub>S/PVA nanocomposite films. *J. Mol. Struct.* **1163**, 442–448 (2018)
- Mohammed, G., El Sayed, A.M., Morsi, W.M.: Spectroscopic, thermal, and electrical properties of MgO/polyvinyl pyrrolidone/ polyvinyl alcohol nanocomposites. *J. Phys. Chem. Solids* **115**, 238–247 (2018)
- Mohammed Kadim, A., Dheyaa Abdulkareem, A., Jawad Kadhim Alrubaie, A., Haneen Abass, K.: Formation of PVA-PMMA-PAAm blend with various content of dextrin for drug delivery application. *Mater. Today Proc.* **80**, 2474–2479 (2023)
- Muhammad, F.F., Aziz, S.B., Hussein, S.A.: Effect of the dopant salt on the optical parameters of PVA:NaNO<sub>3</sub> solid polymer electrolyte. *J. Mater. Sci. Mater. Electron.* **26**, 521–529 (2015)
- Nasrallah, D.A., Ibrahim, M.A.: Enhancement of physico-chemical, optical, dielectric and antimicrobial properties of polyvinyl alcohol/carboxymethyl cellulose blend films by addition of silver doped hydroxyapatite nanoparticles. *J. Polym. Res.* **29**, 86 (2022)
- Omkaram, I., Sreekanth Chakradhar, R.P., Lakshmana Rao, J.: EPR, optical, infrared and Raman studies of VO<sup>2+</sup> ions in polyvinylalcohol films. *Phys. B Cond. Matt.* **388**, 318–325 (2007)
- Qasrawi, A.F., Shukri Ahmad, M.M.: Optoelectrical properties of polycrystallineβ -GaSe thin films. *Cryst. Res. Technol.* **41**, 364–370 (2006)

- Rajesh, K., Crasta, V., Rithin Kumar, N.B., Shetty, G., Rekha, P.D.: Structural, optical, mechanical and dielectric properties of titanium dioxide doped PVA/PVP nanocomposite. *J. Polym. Res.* **26**, 99 (2019a)
- Rajesh, K., Crasta, V., Rithin Kumar, N.B., Shetty, G., Sangappa, Y., Kudva, J., Vijeth, H.: Effect of MoO<sub>3</sub> nanofiller on structural, optical, mechanical, dielectric and thermal properties of PVA/PVP blend. *Mater. Res. Innovat.* **24**, 270–278 (2019b)
- Rezeki, Y.A., Wahyuni, N., Munir, M.M., Khairurrijal, K.: Synthesis of polyvinylpyrrolidone/mangosteen pericarp extract (MPE) fibered particles using electrospray. *J. Phys. Conf. Ser.* **1282**, 012033 (2019)
- Safo, I.A., Werheid, M., Dosche, C., Oezaslan, M.: The role of polyvinylpyrrolidone (PVP) as a capping and structure-directing agent in the formation of Pt nanocubes. *Nanoscale Adv.* **1**, 3095–3106 (2019)
- Salem, A.M., Selim, M.S.: Structure and optical properties of chemically deposited Sb<sub>2</sub>S<sub>3</sub> thin films. *J. Phys. D Appl. Phys.* **34**, 12–17 (2001)
- Subramanian, S.: C.I. P, P.P. D, Influence of polyaniline doping concentration in (Bi<sub>0.5</sub>Sb<sub>0.5</sub>)<sub>2</sub>S<sub>3</sub> thin polycrystalline films on structural, electrical and optical properties. *J. Non-Crystall. Solids* **356**, 1173–1179 (2010)
- Sudha Kamath, M.K., Harish Kumar, H.G., Chandramani, R., Radhakrishna, M.C.: PVP Influence on PVA crystallinity and optical band gap. *Arch. Phys. Res.* **6**, 18–21 (2015)
- Sudheesh, P., Sharafudeen, K.N., Vijayakumar, S., Chandrasekharan, K.: Preparation and study of nonlinear optical response of Ag and Au nano particles doped PVA/PVP thin films. *J. Opt.* **40**, 193–197 (2011)
- Sultanova, N.G., Kasarova, S.N., Nikolov, I.D.: Characterization of optical properties of optical polymers. *Opt. Quant. Electron.* **45**, 221–232 (2012)
- Teleb, N.H., Abd El-Ghany, W.A., Salem, A.M.: Synthesis, structure and optical properties of Ge<sub>26</sub>In<sub>x</sub>Se<sub>74-x</sub> thin films for photonic applications. *J. Non-Crystall. Solids* **572**, 121103 (2021)
- Uma Maheshwari, S., Govindan, K., Raja, M., Raja, A., Pravin, M.B.S., Vasanth Kumar, S.: Preliminary studies of PVA/PVP blends incorporated with HAp and beta-TCP bone ceramic as template for hard tissue engineering. *Bio-Med. Mater. Eng.* **28**, 401–415 (2017)
- Wemple, S.H., DiDomenico, J.: Behavior of the electronic dielectric constant in covalent and ionic materials. *Phys. Rev. B* **3**, 1338–1351 (1971)
- Zidan, H.M., El-Ghamaz, N.A., Abdelghany, A.M., Lotfy, A.: Structural and electrical properties of PVA/PVP blend doped with methylene blue dye. *Int. J. Electrochem. Sci.* **11**, 9041–9056 (2016)
- Zidan, H.M., Abdelrazek, E.M., Abdelghany, A.M., Tarabiah, A.E.: Characterization and some physical studies of PVA/PVP filled with MWCNTs. *J. Market. Res.* **8**, 904–913 (2019)

**Publisher's Note** Springer Nature remains neutral with regard to jurisdictional claims in published maps and institutional affiliations.